Metabolism

Molecular Cancer Research

PPARδ Reprograms Glutamine Metabolism in Sorafenib-Resistant HCC

Mi-Jin Kim[1,2], Yeon-Kyung Choi[1,3], Soo Young Park[1], Se Young Jang[1], Jung Yi Lee[3], Hye Jin Ham[3], Byung-Gyu Kim[3], Hui-Jeon Jeon[3], Ji-Hyun Kim[1,2], Jung-Guk Kim[1], In-Kyu Lee[1,2,3], and Keun-Gyu Park[1,2,3]

Abstract

The tyrosine kinase inhibitor sorafenib is the only therapeutic agent approved for the treatment of advanced hepatocellular carcinoma (HCC), but acquired resistance to sorafenib is high. Here, we report metabolic reprogramming in sorafenib-resistant HCC and identify a regulatory molecule, peroxisome proliferator–activated receptor-δ (PPARδ), as a potential therapeutic target. Sorafenib-resistant HCC cells showed markedly higher glutamine metabolism and reductive glutamine carboxylation, which was accompanied by increased glucose-derived pentose phosphate pathway and glutamine-derived lipid biosynthetic pathways and resistance to oxidative stress. These glutamine-dependent metabolic alterations were attributed to PPARδ, which was upregulated in sorafenib-resistant HCC cells and human HCC tissues. Furthermore, PPARδ contributed to increased proliferative capacity and redox homeostasis in sorafenib-resistant HCC cells. Accordingly, inhibiting PPARδ activity reversed compensatory metabolic reprogramming in sorafenib-resistant HCC cells and sensitized them to sorafenib. Therefore, targeting compensatory metabolic reprogramming of glutamine metabolism in sorafenib-resistant HCC by inhibiting PPARδ constitutes a potential therapeutic strategy for overcoming sorafenib-resistance in HCC.

Implications: This study provides novel insight into the mechanism underlying sorafenib resistance and a potential therapeutic strategy targeting PPARδ in advanced hepatocellular carcinoma. *Mol Cancer Res; 15(9); 1230–42. ©2017 AACR.*

Introduction

Hepatocellular carcinoma (HCC) is one of the most common and fatal malignancies worldwide (1). HCC is usually diagnosed at an advanced stage, meaning that surgical resection is not possible and the response to chemotherapy is poor (2). Although sorafenib, a multikinase inhibitor, has received approval for the treatment of advanced HCC, the extension of overall survival and treatment response rates is usually quite low (3). Moreover, a considerable number of patients develop acquired resistance to the drug and relapse within a few months, even when the initial response is satisfactory (4). Therefore, it is important to identify the molecular mechanisms underlying sorafenib resistance and the molecular targets that will allow us to overcome sorafenib resistance and improve response rates to sorafenib in advanced HCC.

Sorafenib targets the Raf-1, B-Raf, and receptor tyrosine kinases such as VEGF receptor, platelet-derived growth factor receptor, and c-Kit, thereby inducing apoptosis and inhibiting cell proliferation and tumor angiogenesis (5). However, the drug may activate several additional pathways, including PI3K/Akt and JAK/STAT, which may lead to sorafenib resistance (6). Clinical trials assessed the above-mentioned molecular targeting agents in combination with sorafenib; unfortunately, the chosen end-point was not reached due to nonsuperiority or systemic toxicity (7). Therefore, alternative approaches to overcoming these barriers and improving therapeutic efficacy are required. Emerging evidence suggests that sorafenib has kinase-independent effects, such as compensatory metabolic reprograming of HCC cells, which play a critical role in the development of drug resistance (8). Metabolic reprogramming is a hallmark of cancer, and recent studies highlight the pivotal role of metabolic flexibility in cancer cells (9). Moreover, the altered metabolic characteristics of cancer cells, such as dysregulated aerobic glucose metabolism, glutaminolysis, and fatty acid synthesis, are associated with therapeutic resistance in cancer cells (9). In this respect, identifying the target molecules that modulate compensatory metabolic reprogramming in sorafenib-resistant HCC cells might be a promising strategy for improving responses to sorafenib and overcoming drug resistance.

A growing body of evidence suggests that several nuclear receptors are upregulated in various cancers and are responsible for the development of drug resistance (10), and that some

[1]Department of Internal Medicine, Kyungpook National University School of Medicine, Daegu, Republic of Korea. [2]Research Institute of Aging and Metabolism, Kyungpook National University School of Medicine, Daegu, Republic of Korea. [3]Leading-edge Research Center for Drug Discovery and Development for Diabetes and Metabolic Disease, Kyungpook National University Hospital, Daegu, Republic of Korea.

M.-J. Kim, Y.-K. Choi, and S.Y. Park contributed equally to this article.

Note: Supplementary data for this article are available at Molecular Cancer Research Online (http://mcr.aacrjournals.org/).

Corresponding Authors: Keun-Gyu Park, Kyungpook National University School of Medicine, 130 Dongdeok-ro, Jung-gu, Daegu 41944, South Korea. Phone.: 82-53-200-3159; Fax: 82-53-420-2046; E-mail: kpark@knu.ac.kr; and In-Kyu Lee, Phone.: 82-53-420-5564; Fax: 82-53-420-2046; E-mail: leei@knu.ac.kr

doi: 10.1158/1541-7786.MCR-17-0061

AACR

of them are involved in regulating nutrient metabolism (11). Peroxisome proliferator–activated receptor (PPAR) δ (also known as PPARβ) plays an important role in energy homeostasis by modulating glucose and lipid metabolism (12, 13). In addition to its metabolic role, PPARδ is overexpressed in human cancers and initiates and accelerates tumor growth by upregulating VEGF expression and promoting cell survival through activated PI3K-Akt signaling (14). With respect to stress-induced cell death, activation of PPARδ increases keratinocyte survival upon growth factor deprivation and anoikis via downregulation of PTEN expression (15), which drives resistance to anticancer therapeutics (16). Thus, it is speculated that increased PPARδ activity may contribute to dysregulated metabolism and drug resistance in cancer cells. However, the relationship between PPARδ, dysregulated metabolism, and sorafenib-resistant HCC is unclear.

Therefore, the aims of this study were to identify the mechanism underlying compensatory metabolic reprogramming in HCC cells in response to prolonged exposure to sorafenib, and to elucidate the role of PPARδ in sorafenib resistance. We also examined whether modulating PPARδ activity has the potential avenues to overcome sorafenib resistance.

Materials and Methods

Cell lines and cell culture

Human HCC Huh7 and SK-Hep-1 cells were obtained from the American Type Culture Collection. Sorafenib-resistant Huh7 (Huh7-R) and SK-Hep-1 (SK-H-R) cells were generated by growing parental cells in the presence of increasing concentrations (up to a maximum concentration of 10 μmol/L) of sorafenib for 8 months. Initially, cell numbers were markedly reduced, and for the following 2 months, the surviving cells were passaged approximately once every 15 days. After resistant cells were established, they were continuously cultured in the presence of sorafenib. Huh7, Huh7-R, SK-Hep-1, and SK-H-R cells were cultured in DMEM (Biological Industries) supplemented with 10% FBS and 1% penicillin/streptomycin. For the glutamine deprivation experiments, cells were incubated in glutamine-free DMEM supplemented with 10% dialyzed FBS. Viable cells were counted using a hemocytometer after trypan blue staining.

Chemicals

Sorafenib was purchased from Cayman Chemical. The glutaminase (GLS) 1 inhibitor, bis-2-(5-phenylacetamido-1,2,4-thiadiazol-2-yl)ethyl sulfide (BPTES), dichloroacetate (DCA), and dimethyl 2-oxoglutarate (DM-αKG) were obtained from Sigma.

Immunoblot analysis

Cells were incubated on ice for 30 minutes in IPH lysis buffer [50 mmol/L Tris (pH 8.0), 150 mmol/L NaCl, 5 mmol/L EDTA, 0.1 mmol/l phenylmethylsulfonyl fluoride, and 0.5% NP-40] containing a protease inhibitor cocktail (Sigma), and dithiothreitol and lysates were clarified by centrifugation at 12,000 × *g* for 10 minutes. Supernatants were collected, and the protein concentration was measured using the Bio-Rad protein assay (Bio-Rad). Cell lysates were resolved by SDS-PAGE and transferred to a PVDF membrane (Millipore Corporation). The membrane was incubated in blocking buffer, followed by primary antibodies as indicated. The membrane was then washed and incubated with a horseradish peroxidase–conjugated secondary antibody (Santa Cruz Biotechnology). Immunoreactive proteins were visualized by chemiluminescence (UVITec), according to the manufacturer's instructions. The following antibodies were used for immunoblotting: cleaved caspase-3, PARP, glucose-6-phosphate dehydrogenase (G6PD; Cell Signaling Technology), sterol regulatory element-binding protein-1 (BD Biosciences), pyruvate dehydrogenase kinase 1 (PDK1; Enzo Life Sciences International), phosphorylated PDHe1α (Calbiochem), PPARδ (Abcam), GLS1 (Proteintech), and actin (Sigma). Band intensity was quantified using ImageJ and normalized to the band intensity of β-actin.

Measurement of the NADPH/$NADP^+$ ratio

The NADPH/$NADP^+$ ratio in HCC cells was assayed using a NADPH/$NADP^+$ Quantification Colorimetric kit (BioVision), according to the manufacturer's instructions, and normalized against the control.

Measurement of the glutathione/glutathione disulfide ratio

The total glutathione (GSH) concentration was determined by measuring the rate of 5-thio-2-nitrobenzoic acid formation. Glutathione disulfide (GSSG) was measured in a 5,5-dithiobis (2-nitrobenzoic acid) (DTNB)–GSSG reductase recycling assay after removal of GSH from 2-vinylpyridine. Total GSH and GSSG levels were measured by monitoring the change in OD at 412 nm for 1 minutes at 37°C.

Annexin V–FITC/propidium iodide staining

The percentage of cells undergoing apoptosis was measured using an Annexin V apoptosis detection kit (BD Biosciences), according to the manufacturer's protocol. Briefly, cells were trypsinized, washed twice with PBS, and fixed with absolute 70% EtOH for at least 30 minutes at 4°C. The fixed cells were then washed twice with PBS. After washing, cells were incubated for 15 minutes with FITC-conjugated Annexin and propidium iodide (PI) in binding buffer (BD Biosciences) in the dark. Annexin V and PI binding was measured within 1 hour by flow cytometry. Data were acquired using a BD Accuri C6 flow cytometer (BD Bioscience) and analyzed using either the Accuri C6 analysis program (BD Biosciences) or FlowJo software (FlowJo, LLC.).

siRNA transfection and adenovirus infection

Huh7-R cells were transfected simultaneously with human PPARδ-siRNA and a control siRNA duplex (Bioneer Corporation) using Lipofectamine RNAiMAX, according to the manufacturer's instructions. At 24 hours after transfection, cells were incubated for 24 hours in medium containing 10% FBS. Huh7 and SK-Hep-1 cells were infected with an adenovirus expressing PPARδ (Ad-PPARδ; VECTOR BIOLABS) for 24 hours in serum-free DMEM media to induce overexpression of PPARδ.

^{13}C-Isotopomer labeling studies

Cells were washed with glucose- or glutamine-free DMEM medium (D5030; Sigma-Aldrich) supplemented with glutamine (4 mmol/L) or glucose (25 mmol/L) and incubated with 25 mmol/L of [U-$^{13}C_6$] glucose (660663; Sigma-Aldrich) or 4 mmol/L [U-$^{13}C_5$, $^{15}N_2$] glutamine (607983; Sigma-Aldrich) in DMEM medium for 24 hours.

Metabolite extraction

Cells were washed with 3 mL of ice-cold 0.9% NaCl (two times) and then collected in an Eppendorf tube (17). Cells were resuspended with 200 μL of ice-cold metabolite extraction solution [methanol:water (1:1, v/v) + 6 μmol/L internal standard] and then mixed with 200 μL of chloroform. After incubation on ice for 1 hour, metabolite samples were collected by centrifugation at 13,000 rpm for 5 minutes. All the upper phase was lyophilized and resuspended in 300 μL of water containing 0.1% formic acid prior to the LC-MS/MS analysis.

LC-MS/MS analysis

Analytes were separated on a pentafluorophenyl column (100 mm × 2.1 mm, 3 μm) or a Mastro C18 (150 mm × 2.1 mm, 3 μm) column by gradient elution using HPLC Nexera coupled to a LCMS-8060 mass spectrometer (Shimadzu). The LC-MS/MS analysis was performed as described previously (18). Briefly, the mobile phase consisted of water-acetonitrile (0.1% formic acid) or methanol at a flow rate of 0.3 mL/min. Q3 selected ion monitoring (SIM) scan mode was used to obtain target metabolite isotopomer information, and raw spectrum intensity data of which were extracted from within a retention time range of each multiple reaction monitoring scan performed simultaneously. Subsequently, ^{13}C-MIDs (mass isotopomer distributions) were determined and corrected for natural isotope abundance from the SIM scan data of the target metabolite isotopomer.

Animal experiments

Experimental procedure 1

To examine the effects of sorafenib against established tumors, 6-week-old athymic male BALB/c nude (nu/nu) mice ($n = 9$, Japan SLC, Inc.) were injected s.c. with Huh7 cells (6×10^6, left flank) and Huh7-R cells (6×10^6, right flank). Mice were then treated by intraperitoneal injection of sorafenib (10 mg/kg) or a vehicle control (DMSO in PBS) every day for 21 days, starting 14 days after intraperitoneal injection of Huh7 and Huh7-R cells. Tumor volume [length × width^2 × 0.5 (mm^3)] was measured every 3 days using digital calipers. All animal procedures were approved by the Institutional Animal Care and Use Committee of Kyungpook National University.

Experimental procedure 2

Huh7 cells or Huh7-R cells (6×10^6) were injected s.c. into the right flank of 6-week-old athymic male BALB/c nude (nu/nu) mice. Mice were then randomized into three groups ($n = 9$ per group): (1) Huh7 tumors treated with sorafenib (10 mg/kg); (2) Huh7-R tumors treated with sorafenib (10 mg/kg); and (3) Huh7-R tumors treated with sorafenib (10 mg/kg) plus GSK0660 (10 mg/kg). When the tumor reached an average volume of 100 mm^3, the mice were treated by intraperitoneal injection of the indicated drugs or a vehicle control (DMSO in PBS) every day for 12 days. Tumor volume was measured every 3 days after injection of the chemical agent. All animal procedures were approved by the Institutional Animal Care and Use Committee of Kyungpook National University.

Histologic and immunohistochemical analysis

Tumor tissues were collected, fixed with PBS containing 4% paraformaldehyde, and embedded in paraffin. Serial (4 μm) sections were subjected to hematoxylin and eosin staining using standard procedures. For immunohistochemical analysis, deparaffinized sections were incubated with primary antibodies (anti-PPARδ, anti-GLS1, anti-PDK1, anti–p-PDHe1α, or anti–Ki-67), followed by a horseradish peroxidase–conjugated anti-mouse IgG secondary antibody (Dako), according to the manufacturer's instructions. The intensity of positive staining per unit area was calculated using MetaMorph software (version 4.6, Universal Imaging Corporation). For the TUNEL assay, tumor sections were stained using the In Situ Cell Death Detection Kit, Fluorescein (Roche Applied Science).

Patients and specimens

The protein levels of PPARδ and GLS1 in tumor tissues taken from 5 HCC patients who underwent ultrasound-guided needle biopsy at the Kyungpook National University Hospital in Daegu, Korea, in 2014 and 2015 were measured by Western blotting. To verify changes in protein levels in response to sorafenib, biopsies were performed both before and after treatment. In addition, to compare changes in PPARδ and GLS1 protein levels as the cancer progressed, tumor tissues at different tumor–node–metastasis (TNM) stages were obtained from 24 patients ($n = 6$ per stage) who underwent surgical resection (stages I, II, and III) or ultrasound-guided needle biopsy (stage IV) at the Kyungpook National University Hospital in Daegu, Korea, from 2012 to 2015. All patients were staged using the American Joint Committee on Cancer (AJCC 2010, 7th edition) TNM staging system (19).

Ethics statement

This study protocol was approved by the Institutional Review Board of Kyungpook National University Hospital (IRB nos. KNUH 2014-04-056 and KNUMCBIO 12-1007). Written informed consent was obtained from each patient.

Statistical analysis

Data were examined using the Student t test and expressed as the mean ± SEM of at least three independent experiments. The association between protein expression and different tumor stage was analyzed using the Kruskal–Wallis test; $P < 0.05$ was considered statistically significant.

Results

Sorafenib-resistant HCC cells are highly proliferative and resistant to oxidative stress

The establishment of sorafenib-resistant cells was evaluated by FACS analysis and by measurement of cleaved caspase-3 and PARP. FACS analysis revealed that sorafenib induced significant death in Huh7 cells but did not affect Huh7-R cells (Fig. 1A). The levels of cleaved caspase-3 and PARP confirmed establishment of sorafenib-resistant Huh7-R and SK-H-R cells (Fig. 1B; Supplementary Fig. S1A and S1B). In addition, Huh7-R and SK-H-R cells were highly proliferative compared with parental cells regardless of the presence/absence of sorafenib (Fig. 1C). To characterize the metabolic reprogramming in sorafenib-resistant HCC cells, we examined two critical steps involved in glucose oxidation and glutaminolysis, along with two important biosynthetic pathways, namely, the pentose phosphate and lipid biosynthetic pathways. We found that the levels of PDK1, phosphorylated PDHe1α, and

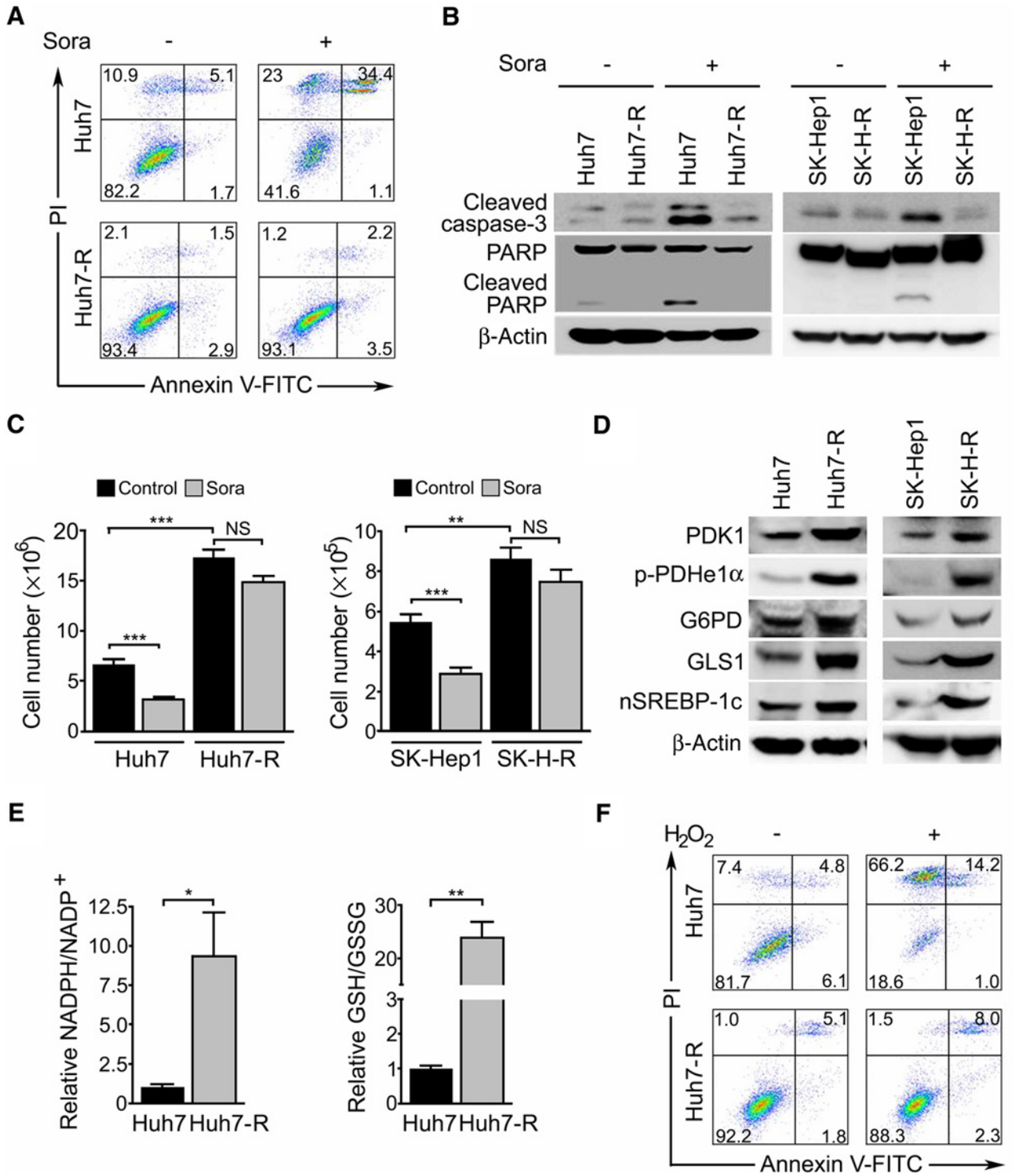

Figure 1.

Metabolic reprogramming of sorafenib-resistant HCC cells. **A,** Sorafenib-resistant Huh7 (Huh7-R) cells and parental (Huh7) cells were incubated with 10 μmol/L sorafenib and subjected to flow cytometry. **B,** Western blot analysis of cleaved caspase-3 and PARP levels in sorafenib-sensitive HCC (Huh7 and SK-Hep1) and -resistant HCC (Huh7-R and SK-H-R) cells in the presence/absence of sorafenib for 24 hours. **C,** Growth of sorafenib-sensitive (Huh7 and SK-Hep1) and -resistant HCC (Huh7-R and SK-H-R) cells in the presence/absence of sorafenib for 24 hours. **D,** Western blot analysis of the indicated protein levels in sorafenib-sensitive HCC (Huh7 and SK-Hep1) and -resistant HCC (Huh7-R and SK-H-R) cells. **E,** Measurement of the relative $NADPH/NADP^+$ (left) and GSH/GSSG (right) ratios in Huh7 and Huh7-R cells. **F,** Cells were incubated with 500 μmol/L H_2O_2 for 15 minutes, and cell death was quantified by FACS analysis of Annexin V/PI fluorescence. Data are expressed as the mean ± SEM of three independent experiments. NS, not significant; *, $P < 0.05$; **, $P < 0.01$; and ***, $P < 0.001$.

G6PD were higher in Huh7-R and SK-H-R cells than in their respective parental lines, suggesting reduced conversion of pyruvate to acetyl-coA and a concomitant shift toward the pentose phosphate pathway in sorafenib-resistant HCC cells (Fig. 1D; Supplementary Fig. S1C and S1D). In addition, levels of GLS1 and the nuclear form of SREBP-1 were higher in Huh7-R and SK-H-R cells than in parental cells (Fig. 1D). Taken together, these data suggest that sorafenib-resistant HCC cells can utilize glucose- and glutamine-derived intermediates as precursors to meet the demands imposed by accelerated proliferation. Given that glutamine supports redox homeostasis by maintaining NADPH-dependent GSH, we next measured the NADPH/$NADP^+$ and GSH/GSSG ratios in Huh7-R cells. As shown in Fig. 1E, the NADPH/$NADP^+$ ratio in Huh7-R cells was more than 8-fold higher, and the GSH/GSSG ratio was 25-fold higher, than that in Huh7 cells. The capacity of Huh7-R cells to resist oxidative stress was evaluated by treatment with hydrogen peroxide. As expected, Huh7-R cells were markedly more resistant to exogenous oxidative stress (Fig. 1F). Altogether, these data suggest that increased glutamine metabolism supports the survival of sorafenib-resistant HCC cells via the NADPH-dependent GSH redox system.

Sorafenib-resistant HCC cells exhibit higher reductive glutamine metabolism

To quantify the contribution of glutamine metabolism to the proliferation of sorafenib-resistant HCC cells, we performed a stable isotope flux study using labeled $^{13}C_5$ glutamine (Fig. 2A). We found that the M+5 glutamate level was

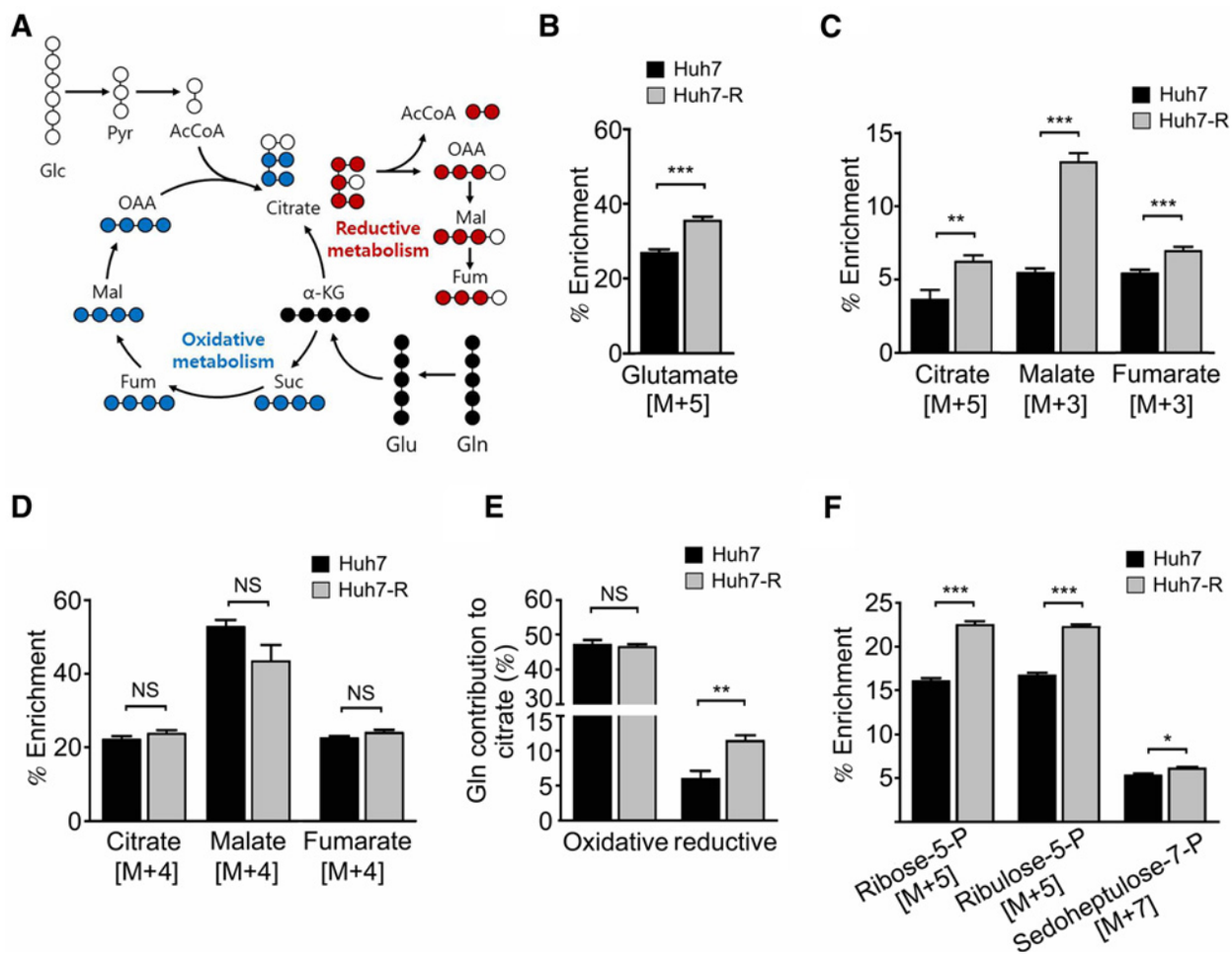

Figure 2.

Sorafenib-resistant HCC cells showed enhanced reductive glutamine metabolism and pentose phosphate pathway. **A–E,** Huh7 and Huh7-R cells were grown in $^{13}C_5$ and $^{15}N_2$-glutamine medium. The isotopologue distributions were determined by LC-MS. **A,** Schematic of carbon atom transitions using $^{13}C_5$ glutamine. Black color indicates the labeled carbon of glutamine before entering the TCA cycle. Red color indicates the effect of glutamine on the TCA cycle through reductive carboxylation. **B–D,** Mass isotopologue distributions of glutamate, citrate, malate, and fumarate in Huh7 and Huh7-R cells cultured in $^{13}C_5$ glutamine. **E,** Ratio of glutamine contribution to citrate via oxidative and reductive pathways. Oxidative and reductive contributions to citrate were determined by calculating M4 and M5 citrate percentages, respectively. **F,** Mass isotopologue distributions of ribose-5-phosphate, ribulose-5-phosphate, and sedoheptulose 7-phosphate in Huh7 and Huh7-R cells cultured in $^{13}C_6$ glucose. Data are expressed as the mean ± SEM. NS, not significant; *, $P < 0.05$; **, $P < 0.01$; and ***, $P < 0.001$.

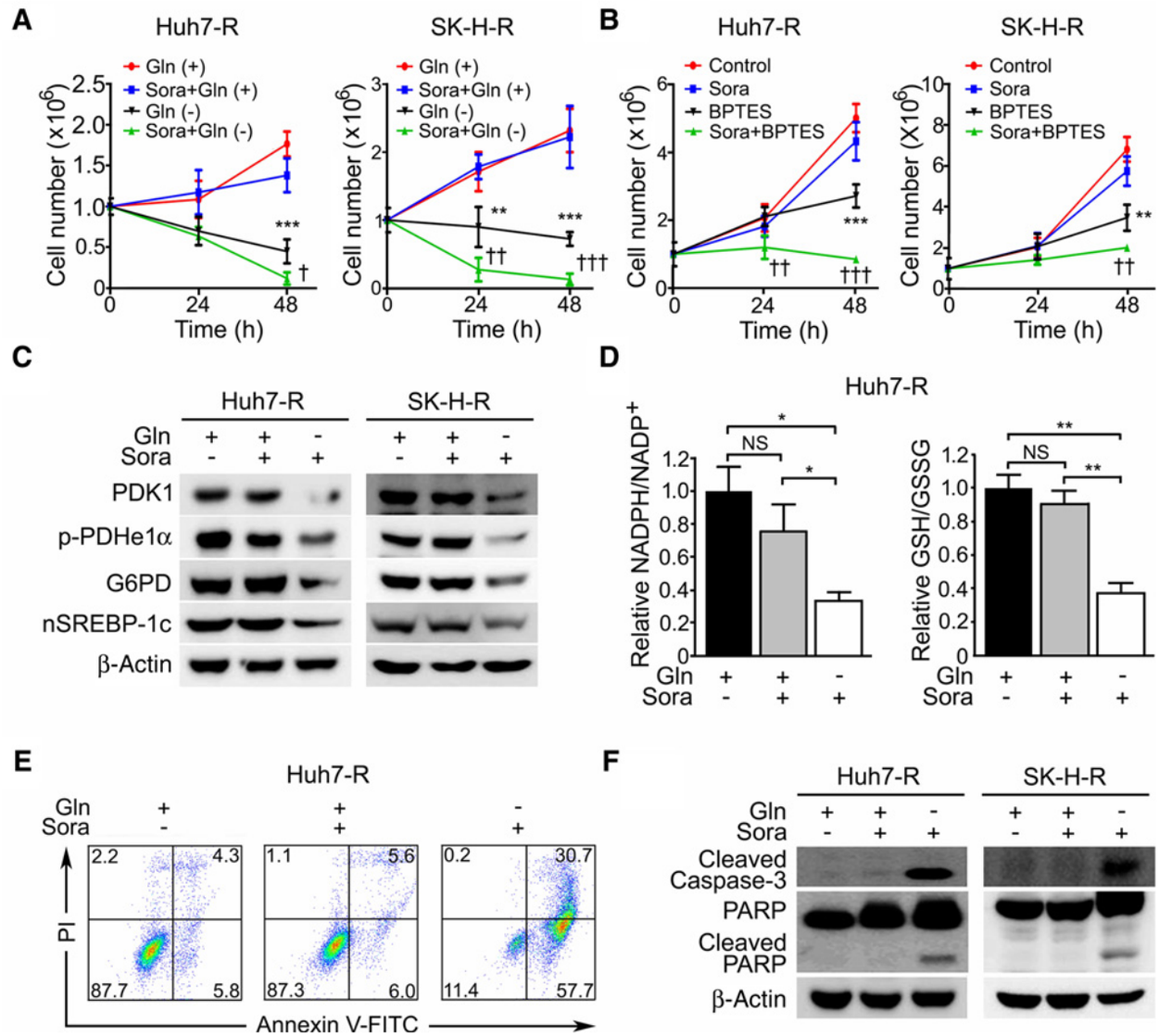

Figure 3.

Inhibition of glutamine metabolism sensitizes sorafenib-resistant HCC cells to sorafenib. **A,** Growth curve analysis of sorafenib-resistant HCC (Huh7-R and SK-H-R) cells treated with sorafenib in the presence/absence of glutamine (Gln). Sorafenib-resistant HCC cells in complete medium without sorafenib were used as a control. Data are expressed as the mean ± SEM of three independent experiments. NS, not significant; *, $P < 0.05$; and ***, $P < 0.001$ vs. the complete medium plus sorafenib group. **B,** Growth curve analysis of sorafenib-resistant HCC (Huh7-R and SK-H-R) cells treated with sorafenib with or without BPTES (10 μmol/L). Data are expressed as the mean ± SEM of three independent experiments. *, $P < 0.05$; **, $P < 0.01$; and ***, $P < 0.001$ vs. the sorafenib alone group. **C–F,** Sorafenib-resistant HCC cells were treated with sorafenib for 24 hours in the presence/absence of glutamine. **C,** Western blot analysis of the indicated proteins in Huh7-R and SK-H-R cells. **D,** Measurement of the relative $NADPH/NADP^+$ (left) and GSH/GSSG (right) ratios in Huh7-R cells under the indicated conditions. Data are expressed as the mean ± SEM of three independent experiments. NS, not significant; *, $P < 0.05$; and **, $P < 0.01$. **E,** Apoptosis of Huh7-R cells, as measured by FACS analysis of Annexin V/PI fluorescence. **F,** Western blot analysis of cleaved caspase-3 and PARP levels in Huh7-R and SK-H-R cells.

significantly higher in Huh7-R cells than in Huh7 cells, indicating enhanced glutaminolysis in sorafenib-resistant HCC cells (Fig. 2B). The levels of M+5 citrate, M+3 malate, and M+3 fumarate, which represent the flux of reductive glutamine metabolism, were significantly higher in Huh7-R cells than in Huh7 cells (Fig. 2C). However, the levels of M+4 citrate, M+4 malate, and M+4 fumarate, which represent the flux of oxidative glutamine metabolism, were not different between Huh7 and Huh7-R cells (Fig. 2D). Consistently, the contribution of reductive glutamine metabolism (but not oxidative glutamine metabolism) to total citrate production was significantly higher in Huh7-R cells than in Huh7 cells, indicating that glutamine-derived glutamate in sorafenib-resistant HCC cells mainly participates in reductive glutamine metabolism rather than in the oxidative pathway (Fig. 2E). Next, we investigated whether changes in the levels of PDK1,

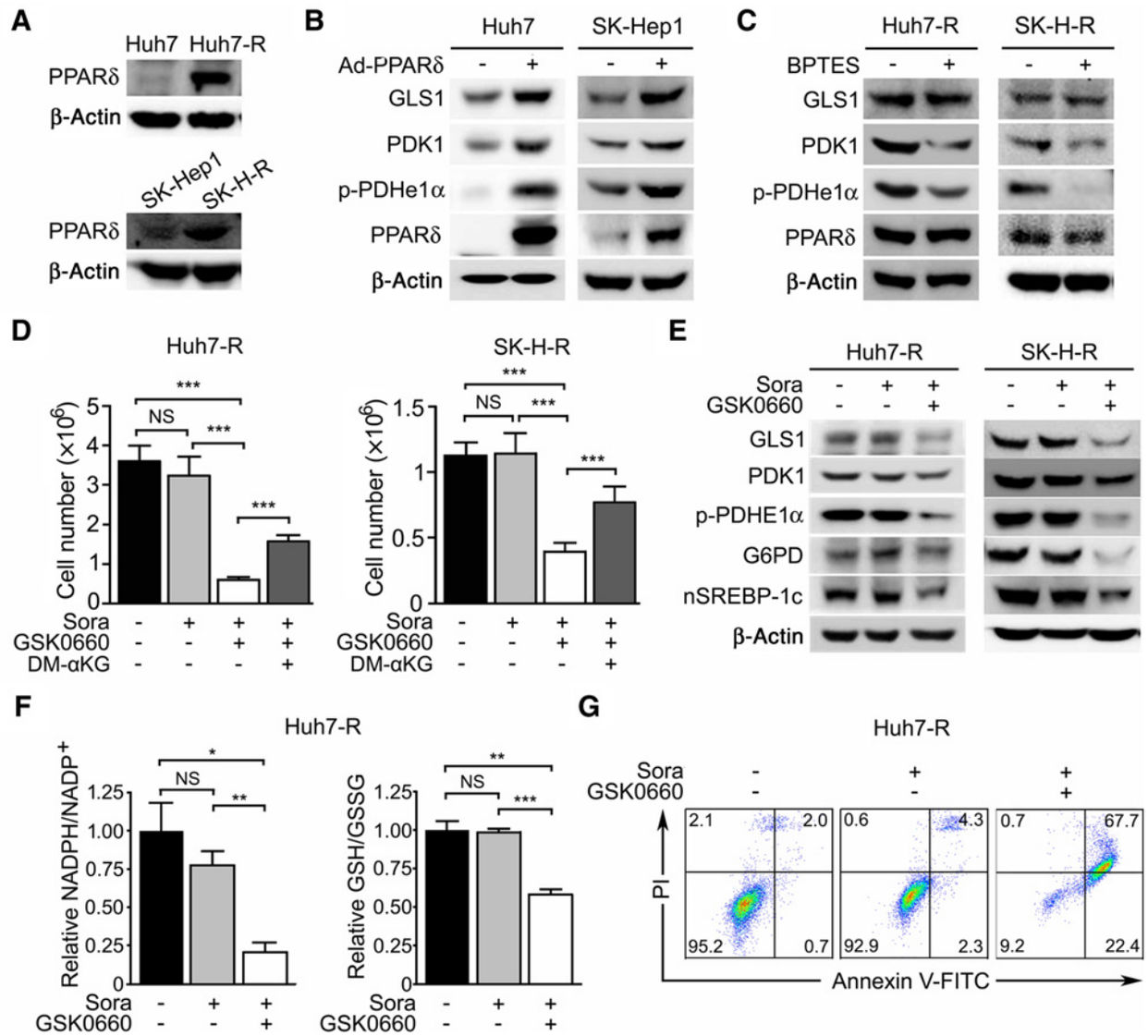

Figure 4.

Contribution of PPARδ to metabolic reprogramming in sorafenib-resistant HCC cells. **A,** Western blot analysis of PPARδ levels in sorafenib-sensitive HCC (Huh7 and SK-Hep1) and -resistant HCC (Huh7-R and SK-H-R) cells. **B,** Western blot analysis showing the effect of PPARδ overexpression on the indicated proteins in Huh7 and SK-Hep1 cells. Cells were infected with adenovirus expressing GFP or PPARδ (MOI of 100, left). **C,** Western blot analysis showing the effect of BPTES (10 μmol/L, left) or DCA (10 mM, right) treatment on the indicated proteins in Huh7-R cells. **D–E,** Huh7-R and SK-H-R cells were treated with sorafenib (10 μmol/L) in the presence/absence of GSK0660 (20 μmol/L) for 24 hours. **D,** Growth of Huh7-R and SK-H-R cells treated with sorafenib in the presence/absence of GSK0660 and DM-αKG (2 mM). **E,** Western blot analysis of the indicated proteins in Huh7-R and SK-HR cells. **F,** Measurement of relative NADPH/$NADP^+$ (left) and GSH/GSSG (right) ratios in Huh7-R cells under the indicated conditions. **G,** Effect of combined treatment with sorafenib plus GSK0660 on apoptosis of Huh7-R cells, as measured by FACS analysis of Annexin V/PI fluorescence. Data are expressed as the mean ± SEM. NS, not significant; *, $P < 0.05$; **, $P < 0.01$; and ***, $P < 0.001$.

phosphorylated PDHe1α, and G6PD in sorafenib-resistant cells actually shifted glucose metabolic flux from glycolysis toward the pentose phosphate pathway by using labeled $^{13}C6$ glucose. Indeed, M+5 ribose-5-phosphate, M+5 ribulose-5-phosphate, and sedoheptulose-7-phosphate were significantly higher in Huh7-R cells than in Huh7 cells (Fig. 2F). Together, these results suggest that sorafenib-resistant HCC cells reprogram their metabolism to provide precursors for rapid cell proliferation.

Inhibiting glutamine metabolism sensitizes sorafenib-resistant HCC cells to sorafenib

The finding of increased glutamine metabolism in sorafenib-resistant HCC cells led us to assess whether targeting glutamine metabolism is a feasible strategy for overcoming sorafenib resistance in HCC. Indeed, sorafenib significantly reduced the proliferation of Huh7-R and SK-H-R cells under conditions of glutamine deprivation, indicating attenuated sorafenib resistance (Fig. 3A). Consistent with this, combined

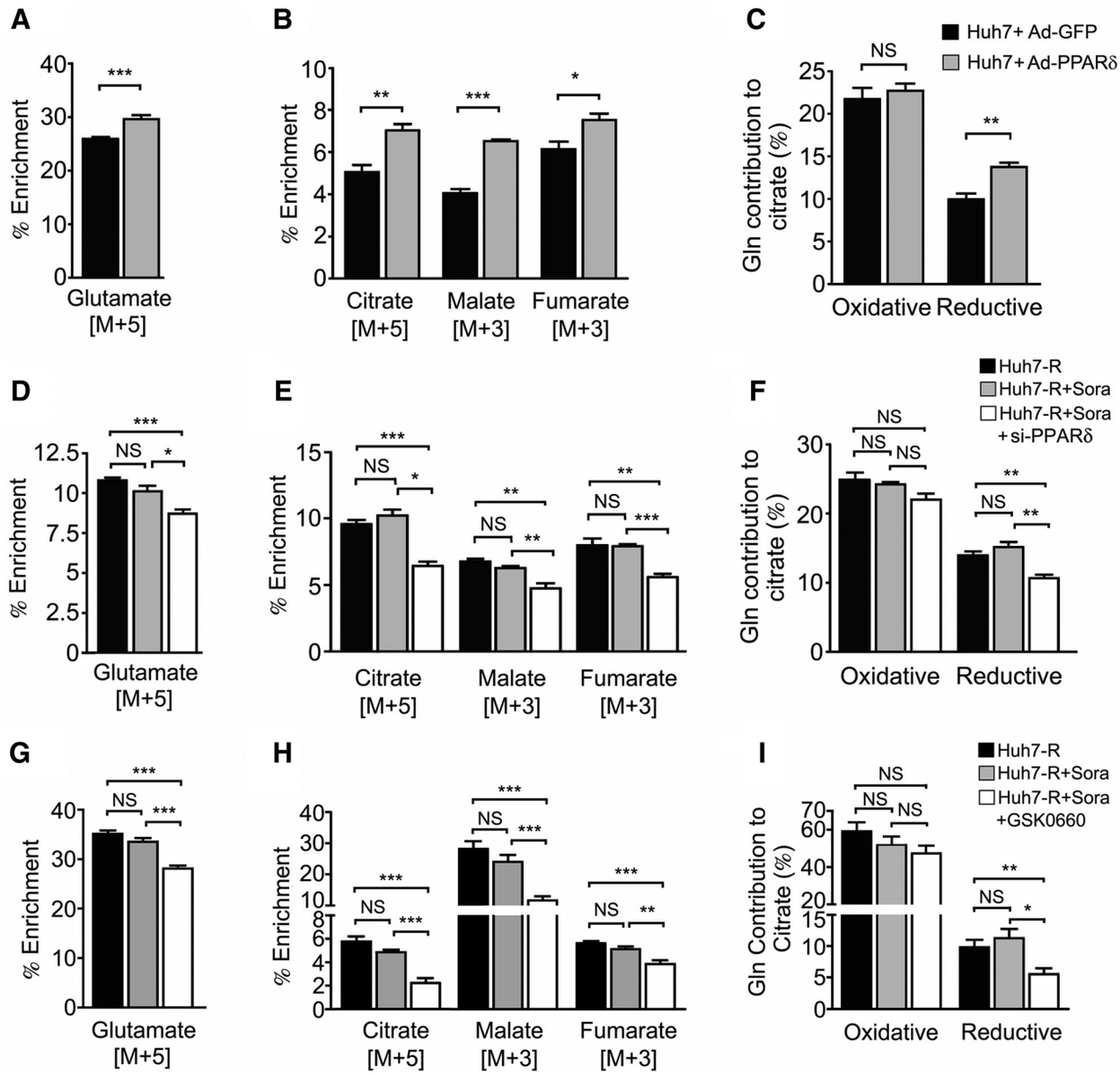

Figure 5.

Role of PPARδ on reductive glutamine metabolism in sorafenib-resistant HCC cells. **A–C,** Huh7 cells were infected with adenovirus-expressing GFP or PPARδ (MOI of 100) and then grown in $^{13}C_5$ and $^{15}N_2$-glutamine medium. The isotopologue distributions were determined by LC-MS. **A** and **B,** Mass isotopologue distributions of glutamate, citrate, malate, and fumarate in Huh7 and Huh7 cells overexpressing PPARδ cultured in $^{13}C_5$ glutamine. **C,** Ratio of glutamine contribution to citrate via oxidative and reductive pathways. Oxidative and reductive contributions to citrate were determined by calculating M4 and M5 citrate percentages, respectively. **D–F,** Huh7-R cells were transfected with scrambled siRNA or siRNA for PPARδ (100 nmol/L). **D** and **E,** Mass isotopologue distributions of glutamate, citrate, malate, and fumarate in Huh7-R and PPARδ-knockdown Huh7-R cells cultured in $^{13}C_5$ glutamine. **F,** Ratio of glutamine contribution to citrate via oxidative and reductive pathways. Oxidative and reductive contributions to citrate were determined by calculating M4 and M5 citrate percentages, respectively. **G–I,** Huh7-R cells were grown in $^{13}C_5$ and $^{15}N_2$-glutamine medium and treated with sorafenib in the presence/absence of GSK0660. **G** and **H,** Mass isotopologue distribution of glutamate, citrate, malate, and fumarate in Huh7-R cells cultured in $^{13}C_5$ glutamine. **I,** Ratio of glutamine contribution to citrate via oxidative and reductive pathways in Huh7-R cells. Data are expressed as the mean ± SEM. NS, not significant; *, $P < 0.05$; **, $P < 0.01$; and ***, $P < 0.001$.

treatment with sorafenib and a chemical inhibitor of GLS1 (BPTES) led to a significant reduction in the number of proliferating sorafenib-resistant HCC cells (Fig. 3B), suggesting that cotreatment with sorafenib and BPTES has therapeutic potential for overcoming sorafenib resistance. Next, we asked whether restricting glutamine metabolism would reverse the upregulated biosynthetic pathway and the increased NADPH/$NADP^+$ and GSH/GSSG ratios in sorafenib-resistant HCC

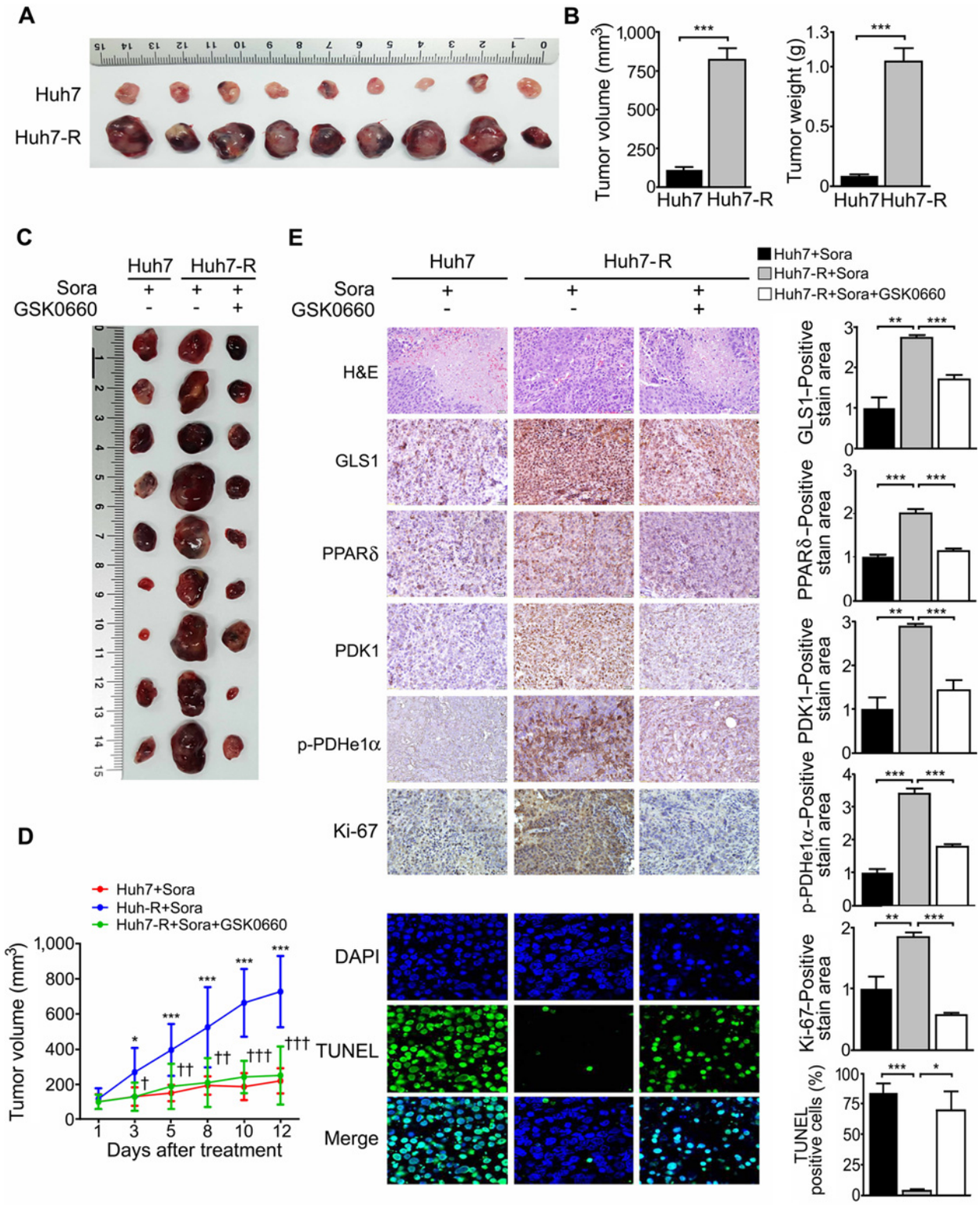

Figure 6.

Effect of a PPARδ inhibitor on tumor growth in a sorafenib-resistant HCC xenograft model. A photograph **(A)** of excised tumor xenografts and (**B**) volume of tumors in mice treated with sorafenib. Each mouse was subcutaneously injected with 6×10^6 Huh7 (left flank) and Huh7-R (right flank) cells. Data are expressed as the mean ± SEM ($n = 9$). ***, $P < 0.001$. (*Continued on the following page.*)

cells. We found that sorafenib reduced the levels of PDK1, phosphorylated PDHe1α, G6PD, and the nuclear form of SREBP-1 in Huh7-R and SK-H-R cells cultured in medium lacking glutamine; this was not the case for cells cultured in complete medium (Fig. 3C; Supplementary Fig. S2A and S2B). Sorafenib also reduced the NADPH/$NADP^+$ and GSH/GSSG ratios in Huh7-R cells under conditions of glutamine deprivation (Fig. 3D). Moreover, under these conditions, sorafenib induced marked apoptosis of sorafenib-resistant HCC cells, which was not observed in parental cells cultured in complete medium (Fig. 3E and F; Supplementary Fig. S2C and S2D). Taken together, these findings indicate that increased glutamine metabolism in sorafenib-resistant HCC cells contributes to increased activation of biosynthetic pathways, greater proliferative capacity, and increased resistance to oxidative stress, suggesting that inhibiting compensatory glutamine metabolism has therapeutic potential for overcoming sorafenib resistance.

PPARδ mediates compensatory glutamine metabolism, and sorafenib resistance is reversed in HCC cells by PPARδ inhibition

To determine the role of PPARδ in the metabolic adaptation observed in sorafenib-resistant cells, we assessed whether PPARδ is upregulated in these cells. Indeed, the levels of PPARδ protein in Huh7-R and SK-H-R cells were markedly higher than those in the parental cells (Fig. 4A; Supplementary Fig. S3A and S3B); thus, we decided to examine the role of PPARδ in metabolic adaptation in sorafenib-resistant cells. Accordingly, we examined the effects of PPARδ activation on the levels of GLS1, PDK1, and phosphorylated PDHe1α in sorafenib-sensitive and -resistant HCC cells. Ad-PPARδ in Huh7 and SK-Hep1 cells increased the levels of GLS1, PDK1, and phosphorylated PDHe1α (Fig. 4B; Supplementary Fig. S3C and S3D). To confirm that changes in glucose metabolism were a consequence of increased glutamine metabolism, we examined the effects of inhibiting either GLS1 or PDK activity on GLS-1 and PDK levels using BPTES or DCA, respectively. The results showed that whereas BPTES reduced PDK1 and phosphorylated PDHe1α levels in Huh7-R and SK-H-R cells (Fig. 4C; Supplementary Fig. S3E and S3F), DCA did not reduce the levels of GLS1, supporting the notion that upregulated PPARδ in sorafenib-resistant cells primarily increases glutamine utilization, which subsequently leads to a reduction in glucose oxidation via upregulation of PDK1 (Supplementary Fig. S3G–S3I).

Next, we examined whether PPARδ inhibition can sensitize sorafenib-resistant HCC cells to sorafenib by inhibiting reductive glutamine metabolism. Combined treatment with sorafenib and GSK0660 led to a marked reduction in both cell proliferation and PDK1 levels in Huh7-R and SK-H-R cells, along with reduced levels of phosphorylated PDHe1α, G6PD, GLS1, and the nuclear form of SREBP-1 (Fig. 4D and E; Supplementary Fig. S4A and S4B). To further explore whether the decrease in sorafenib-resistant cell proliferation induced by GSK0660 is due to limited glutamine metabolism, we treated these cells with the glutamine metabolite, DM-αKG. Indeed, supplementation with DM-αKG significantly rescued the decrease in Huh7-R and SK-H-R cell proliferation under combined treatment with GSK0660 and sorafenib (Fig. 4D). Combination treatment led to a marked reduction in the cellular NADPH/$NADP^+$ and GSH/GSSG ratios, resulting in significant apoptosis of Huh7-R cells (Fig. 4F and G). GSK0660 did not influence the proliferation of Huh7 and SK-Hep1 cells, indicating the reduction of sorafenib-resistant cells is not caused by its toxicity (Supplementary Fig. S4C and S4D).

PPARδ promotes reductive glutamine metabolism in sorafenib-resistant HCC cells

We further investigated whether PPARδ directly contributes to compensatory glutamine metabolism by performing a stable isotope flux study with labeled $^{13}C_5$ glutamine (Fig. 2A). Ad-PPARδ–infected Huh7 cells showed an increase in glutaminolysis (identified by examining the level of M+5 glutamate) and reductive glutamine metabolism (identified by examining the level of M+5 citrate, M+3 malate, and M+3 fumarate), whereas it did not induce a significant change in oxidative glutamine metabolism (identified by examining the levels of M+4 citrate, M+4 malate, and M+4 fumarate; Fig. 5A and B; Supplementary Fig. S4E). The contribution of reductive glutamine metabolism to total citrate production was also significantly increased by overexpression of PPARδ (Fig. 5C).

Next, we found that siRNA-mediated PPARδ silencing attenuated glutaminolysis and reductive carboxylation of glutamine as evidenced by the reduction in the levels of M+5 glutamate and the levels of M+5 citrate, M+3 malate, and M+3 fumarate, respectively, in sorafenib-resistant HCC cells (Fig. 5D and E). Furthermore, knockdown of PPARδ in sorafenib-resistant HCC cells significantly reduced the contribution of reductive glutamine metabolism to total citrate production without affecting the contribution of oxidative glutamine metabolism (Fig. 5F). Consistently, attenuated glutamine metabolism was observed following combined treatment of sorafenib-resistant HCC cells with GSK0660 and sorafenib (Fig. 5G–I), suggesting that PPARδ has an important role in compensatory glutamine metabolism.

Cotreatment with the PPARδ inhibitor and sorafenib inhibits tumor growth *in vivo*

Next, we examined *in vivo* cooperativity between a PPARδ inhibitor and sorafenib in nude mice bearing s.c. Huh7-R xenografts. Consistent with the results of the *in vitro* cell proliferation studies, tumors in mice injected with Huh7-R cells were

(*Continued.*) A photograph **(C)** of excised tumor xenografts and **(D)** growth curves of tumors in mice treated with sorafenib (10 mg/kg) in the presence/absence of GSK0660 (10 mg/kg). Each mouse was subcutaneously injected in the right flank with 6×10^6 Huh7 or Huh7-R cells. Data are expressed as the mean ± SEM ($n = 9$ per group). *, $P < 0.05$ and ***, $P < 0.001$ vs. Huh7 tumors treated with sorafenib; †, $P < 0.05$; ††, $P < 0.01$; and †††, $P < 0.001$ vs. Huh7-R tumors treated with sorafenib. **E,** Representative images of sections of xenografts from mice treated with sorafenib in the presence/absence of GSK0660 and stained with hematoxylin and eosin, or with antibodies against GLS1, PPARδ, PDK1, or phosphorylated PDHe1α (top), or subjected to a TUNEL assay (bottom). All data (obtained by MetaMorph software analysis of positive areas in the tumors) were normalized against the control, and all data in the bar graphs are expressed as the fold increase relative to the control. Data are expressed as the mean ± SEM of three independent measurements. *, $P < 0.05$; **, $P < 0.01$; and ***, $P < 0.001$ vs. the indicated group. Original magnification, ×200.

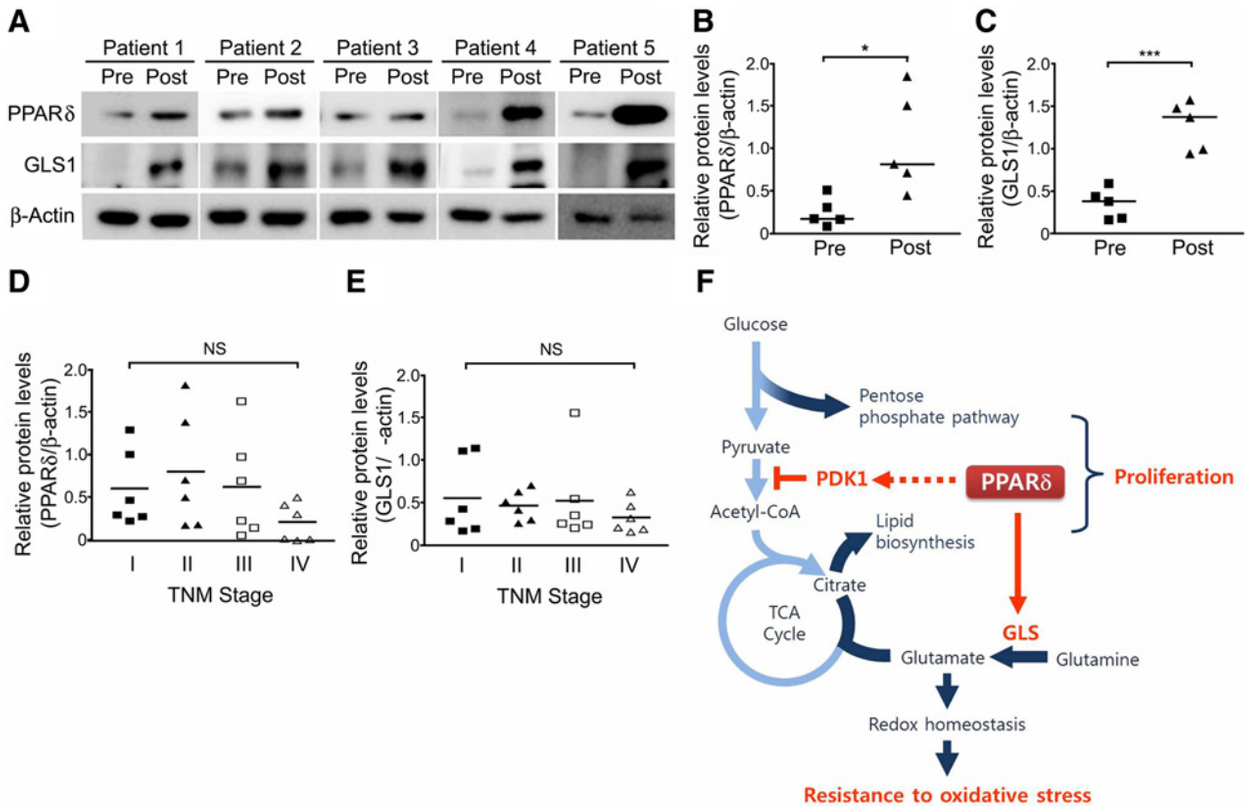

Figure 7.
PPARδ and GLS1 levels are increased in clinically progressed human HCC tissues after sorafenib treatment. **A,** Levels of PPARδ and GLS1 protein in sorafenib-treated human HCC tumors and sorafenib-pretreatment biopsy samples (as measured by Western blotting). **B** and **C,** The integrated optical densities of PPARδ and GLS1 were analyzed and expressed relative to that of actin. **D** and **E,** PPARδ and GLS1 levels in human HCC tissues according to TNM stage were as measured by Western blotting ($n = 6$ for each stage). The integrated optical densities of PPARδ and GLS1 were analyzed and expressed relative to that of actin. **F,** Proposed working model of PPARδ-mediated metabolic reprogramming in sorafenib-resistant cells. NS, not significant; *, $P < 0.05$ and ***, $P < 0.001$.

significantly larger than those in mice injected with Huh7 cells (mean tumor volume: 814.2 vs. 106.3 mm^3, respectively; $P < 0.001$; Fig. 6A and B). Treatment of Huh7-R–bearing mice with sorafenib plus GSK0660 led to a marked reduction in tumor growth when compared with treatment with sorafenib (Fig. 6C and D; Supplementary Fig. S5A). Given that GSK0660 did not affect tumor growth in Huh7-bearing mice (Supplementary Fig. S5B and S5C), GSK0660-induced sensitization of sorafenib-resistant tumors to sorafenib is less likely due to its toxicity. Of note, immunohistochemical analysis revealed that the levels of GLS1, PPARδ, PDK1, and phosphorylated PDHe1α were markedly higher in xenograft tumor tissues, and were attenuated by combined treatment with sorafenib and GSK0660 (Fig. 6E, top). Finally, the number of TUNEL-positive cells was markedly higher in xenograft tumors from mice treated with sorafenib plus GSK0660 (Fig. 6E, bottom). There was no difference in body weight between groups (Supplementary Fig. S5D).

PPARδ and GLS1 levels increase in clinically progressed human HCC tissues after sorafenib treatment

Finally, we examined whether PPARδ and GLS1 levels are upregulated in clinically progressed human HCC tissues after sorafenib treatment. Biopsy specimens from 5 patients with advanced HCC were obtained prior to sorafenib treatment. Biopsy specimens of viable HCC tissues were then obtained from the same individual patients with progressed HCC after sorafenib administration. The levels of PPARδ and GLS1 in sorafenib-exposed human HCC tissues were higher than those observed prior to sorafenib administration (Fig. 7A–C). Considering that all of these patients developed progressive disease after sorafenib treatment, these results support the findings from the *in vitro* and xenograft experiments showing that upregulation of PPARδ expression and glutamine metabolism contribute to sorafenib resistance. To exclude the possibility that upregulation of PPARδ and GLS1 protein levels is a natural consequence of HCC progression, we measured the levels of these proteins in sorafenib-unexposed human HCC tissues at four different TNM stages. The results showed that the protein levels of PPARδ and GLS-1 in human HCC tissues were not associated with HCC progression (Fig. 7D and E). The clinicopathologic characteristics of HCC patients are described in Supplementary Tables S1 and S2.

Discussion

In this study, we examined the metabolic reprogramming responsible for sorafenib resistance in HCC. Sorafenib-resistant

HCC cells exhibited markedly higher glutamine utilization and reductive glutamine metabolism, which drives cell proliferation and maintains redox balance. The increases in glutamine metabolism and reductive glutamine carboxylation in sorafenib-resistant HCC cells were attributed to upregulation of PPARδ (Fig. 7F). Accordingly, inhibition of glutamine metabolism or PPARδ function reversed the metabolic reprogramming in sorafenib-resistant HCC cells and sensitized them to sorafenib. Furthermore, the finding of upregulated PPARδ and GLS1 in sorafenib-exposed human HCC tissues supported *in vitro* and *in vivo* findings.

Several mechanisms are proposed to be responsible for sorafenib resistance in cancer cells, but metabolic adaptation in these cells has not been established (20). Mounting evidence indicates that aggressive proliferation of cancer cells relies on reductive glutamine metabolism, which serves anabolic pathways such as those involved in lipid biosynthesis (21, 22). In line with this, we showed that sorafenib-resistant HCC cells had a greater proliferative capacity than parental cells. Of note, sorafenib-resistant HCC cells showed higher glutamine metabolism and reductive glutamine metabolism, which lead to the upregulation of anabolic pathways that drive rapid cell proliferation, as evidenced by the higher expression of genes involved in pyruvate oxidation (PDK1), fatty acid synthesis (SREBP-1), and the pentose phosphate pathway (G6PD). This finding is consistent with that of previous studies, which suggested that a high proliferative capacity promotes resistance to chemotherapy (23, 24).

Recently, reprogramming of glutamine metabolism has also received increasing attention as a key avenue for circumventing therapeutic resistance in various cancers (25). In support of previous observations, our data show that sorafenib-resistant HCC cells are extremely vulnerable to glutamine deprivation, which is associated with marked reductions in the levels of PDK1, phosphorylated PDHe1α, G6PD, and the nuclear form of SREBP-1. The results indicate that the metabolic reprogramming that drives drug resistance is glutamine-dependent. Glutamine provides precursors for the GSH biosynthesis pathway, and the pentose phosphate pathway plays a critical role in maintaining cellular NADPH levels; both of these pathways are required for the attenuation of ROS (21, 22, 26). An appropriate response to ROS challenge is one of the most important determinants of cell survival in extreme environments such as those encountered during nutrient deprivation or treatment with anticancer drugs (27). Indeed, we observed that sorafenib-resistant HCC cells harbored more NADPH and GSH levels than parental cells; consequently, they were more resistant to oxidative stress-induced apoptosis. We anticipate that metabolic reprogramming in sorafenib-resistant HCC cells helps maintain an abundant supply of NADPH, which acts as a reducing agent during anabolic reactions such as lipogenesis, and maintains the cellular redox balance by reducing GSSG to GSH to prevent ROS-mediated damage.

Although targeting glutamine metabolism effectively inhibits sorafenib-resistant HCC proliferation and induces cell death, the *in vivo* efficacy and toxicity of pharmacologic inhibitors of glutamine metabolism remain largely unknown. Therefore, it is necessary to identify novel targets that act as upstream regulators of glutamine metabolism in sorafenib-resistant HCC cells. A number of studies have suggested that PPARα and PPARγ activation could be used as a target to prevent or treat cancer through both PPAR-dependent and -independent mechanisms (28). In particular, in terms of glutamine metabolism, the PPARγ agonist Troglitazone has been shown to exhibit antitumor activity by suppressing glutamine uptake and incorporation into the TCA cycle (29). By contrast, there is no broad consensus concerning the role of PPARδ in carcinogenesis (28). The present study raises the possibility that PPARδ could serve as a target for overcoming sorafenib resistance because it functions as an upstream regulator of glutamine metabolism.

This study showed that combined treatment of sorafenib-resistant HCC cells with a PPARδ inhibitor and sorafenib markedly reduced GLS-1, PDK1, and G6PD levels. Given that these genes support biosynthetic pathways in proliferating cells, reductions in their levels would attenuate the accelerated proliferation of sorafenib-resistant HCC cells. To the best of our knowledge, this is the first study to show that PPARδ regulates the protein levels of GLS1, PDK1, and G6PD. However, we were unable to obtain evidence to show that PPARδ regulates PDK1, GLS1, and G6PD mRNA expression (data not shown); therefore, a further study is needed to determine whether PPARδ influences the posttranscriptional regulation of these genes.

Notably, inhibition of PPARδ activity recovered sorafenib susceptibility in sorafenib-resistant HCC cells via downregulation of glutamine-dependent reductive carboxylation and biosynthetic pathways. Therefore, our findings underscore the pivotal role of PPARδ in sorafenib resistance in HCC. Importantly, upregulation of PPARδ and GLS1 was detected in post-treatment biopsy specimens taken from HCC patients with progressive disease after sorafenib therapy. Although the number of patient samples analyzed in this study was small, the findings suggest that further studies aimed at understanding the impact of PPARδ and GLS1 on the therapeutic response to sorafenib are warranted.

In conclusion, the data presented herein show that PPARδ-induced compensatory glutamine metabolism contributes to metabolic reprogramming, an essential hallmark that drives cell proliferation and confers resistance to oxidative stress. A pharmacologic inhibitor of PPARδ may be a novel strategy for increasing the sensitivity of HCC to sorafenib; therefore, these findings open the door to novel therapeutic approaches to overcoming sorafenib-resistant HCC.

Disclosure of Potential Conflicts of Interest

No potential conflicts of interest were disclosed.

Authors' Contributions

Conception and design: M.-J. Kim, Y.-K. Choi, S.Y. Park, J.-H. Kim, I.-K. Lee, K.-G. Park

Development of methodology: M.-J. Kim, Y.-K. Choi, H.J. Ham, B.-G. Kim, H.-J. Jeon, J.-H. Kim

Acquisition of data (provided animals, acquired and managed patients, provided facilities, etc.): M.-J. Kim, S.Y. Park, S.Y. Jang

Analysis and interpretation of data (e.g., statistical analysis, biostatistics, computational analysis): M.-J. Kim, Y.-K. Choi, S.Y. Park, J.Y. Lee, H.J. Ham, B.-G. Kim, J.-H. Kim, K.-G. Park

Writing, review, and/or revision of the manuscript: M.-J. Kim, Y.-K. Choi, J.-H. Kim, K.-G. Park

Administrative, technical, or material support (i.e., reporting or organizing data, constructing databases): M.-J. Kim, K.-G. Park

Study supervision: J.-G. Kim, I.-K. Lee, K.-G. Park

Acknowledgments

The specimens used for this study were obtained under IRB-approved protocols (IRB nos. KNUH 2014-04-056 and KNUMCBIO_12-1007). All patients provided written informed consent. The cancer tissues for this study were provided by the Kyungpook National University Hospital Biobank, a member of the National Biobank of Korea, which is supported by the Ministry of Health and Welfare. All samples from the National Biobank of Korea were obtained with informed consent under Institutional Review Board–approved protocols.

Grant Support

This work was supported by grants (NRF-2015R1A2A1A15053422 and NRF-2015R1A2A1A10052745) from the National Research Foundation of Korea, funded by the Ministry of Science, ICT and Future Planning, grants (NRF-2017R1A6A3A04010231) from the National Research Foundation of Korea funded by the Ministry of Education, and grants (HI15C0001 and HI16C1501) from the Korea Health technology R&D Project through the Korea Health Industry Development Institute (KHIDI), funded by the Ministry of Health and Welfare, Republic of Korea.

The costs of publication of this article were defrayed in part by the payment of page charges. This article must therefore be hereby marked *advertisement* in accordance with 18 U.S.C. Section 1734 solely to indicate this fact.

Received February 1, 2017; revised April 25, 2017; accepted May 23, 2017; published OnlineFirst June 5, 2017.

References

1. Yang JD, Roberts LR. Hepatocellular carcinoma: a global view. Nat Rev Gastroenterol Hepatol 2010;7:448–58.
2. Berasain C.Hepatocellular carcinoma and sorafenib: too many resistance mechanisms? Gut 2013;62:1674–5.
3. Llovet JM, Ricci S, Mazzaferro V, Hilgard P, Gane E, Blanc JF, et al. Sorafenib in advanced hepatocellular carcinoma. N Engl J Med 2008; 359:378–90.
4. Villanueva A, Llovet JM. Second-line therapies in hepatocellular carcinoma: emergence of resistance to sorafenib. Clin Cancer Res 2012;18: 1824–6.
5. Wilhelm SM, Carter C, Tang L, Wilkie D, McNabola A, Rong H, et al. BAY 43–9006 exhibits broad spectrum oral antitumor activity and targets the RAF/MEK/ERK pathway and receptor tyrosine kinases involved in tumor progression and angiogenesis. Cancer Res 2004;64: 7099–109.
6. Zhai B, Sun XY. Mechanisms of resistance to sorafenib and the corresponding strategies in hepatocellular carcinoma. World J Hepatol 2013; 5:345–52.
7. Deng GL, Zeng S, Shen H. Chemotherapy and target therapy for hepatocellular carcinoma: new advances and challenges. World J Hepatol 2015; 7:787–98.
8. Liang Y, Zheng T, Song R, Wang J, Yin D, Wang L, et al. Hypoxia-mediated sorafenib resistance can be overcome by EF24 through Von Hippel-Lindau tumor suppressor-dependent HIF-1alpha inhibition in hepatocellular carcinoma. Hepatology 2013; 57:1847–57.
9. Zhao Y, Butler EB, Tan M. Targeting cellular metabolism to improve cancer therapeutics. Cell Death Dis 2013;4:e532.
10. Baek SH, Kim KI. Emerging roles of orphan nuclear receptors in cancer. Annu Rev Physiol 2014;76:177–95.
11. Pearen MA, Muscat GE. Orphan nuclear receptors and the regulation of nutrient metabolism: understanding obesity. Physiology (Bethesda) 2012;27:156–66.
12. Wang YX, Lee CH, Tiep S, Yu RT, Ham J, Kang H, et al. Peroxisome-proliferator-activated receptor delta activates fat metabolism to prevent obesity. Cell 2003;113:159–70.
13. Giordano Attianese GM, Desvergne B. Integrative and systemic approaches for evaluating PPARbeta/delta (PPARD) function. Nucl Recept Signal 2015;13:e001.
14. Wang D, Wang H, Guo Y, Ning W, Katkuri S, Wahli W, et al. Crosstalk between peroxisome proliferator-activated receptor delta and VEGF stimulates cancer progression. Proc Natl Acad Sci U S A 2006;103: 19069–74.
15. Di-Poi N, Tan NS, Michalik L, Wahli W, Desvergne B. Antiapoptotic role of PPARbeta in keratinocytes via transcriptional control of the Akt1 signaling pathway. Mol Cell 2002;10:721–33.
16. Dillon LM, Miller TW. Therapeutic targeting of cancers with loss of PTEN function. Curr Drug Targets 2014;15:65–79.
17. Sapcariu SC, Kanashova T, Weindl D, Ghelfi J, Dittmar G, Hiller K. Simultaneous extraction of proteins and metabolites from cells in culture. MethodsX 2014;1:74–80.
18. Go Y, Jeong JY, Jeoung NH, Jeon JH, Park BY, Kang HJ, et al. Inhibition of pyruvate dehydrogenase kinase 2 protects against hepatic steatosis through modulation of tricarboxylic acid cycle anaplerosis and ketogenesis. Diabetes 2016;65:2876–87.
19. Edge SB, Compton CC. The American Joint Committee on Cancer: the 7th edition of the AJCC cancer staging manual and the future of TNM. Ann Surg Oncol 2010;17:1471–4.
20. Zhao Y, Liu H, Liu Z, Ding Y, Ledoux SP, Wilson GL, et al. Overcoming trastuzumab resistance in breast cancer by targeting dysregulated glucose metabolism. Cancer Res 2011;71:4585–97.
21. Alberghina L, Gaglio D. Redox control of glutamine utilization in cancer. Cell Death Dis 2014;5:e1561.
22. Patra KC, Hay N. The pentose phosphate pathway and cancer. Trends Biochem Sci 2014;39:347–54.
23. Guo D, Reinitz F, Youssef M, Hong C, Nathanson D, Akhavan D, et al. An LXR agonist promotes glioblastoma cell death through inhibition of an EGFR/AKT/SREBP-1/LDLR-dependent pathway. Cancer Discov 2011;1: 442–56.
24. Riganti C, Gazzano E, Polimeni M, Aldieri E, Ghigo D. The pentose phosphate pathway: an antioxidant defense and a crossroad in tumor cell fate. Free Radic Biol Med 2012;53:421–36.
25. Kamata S, Kishimoto T, Kobayashi S, Miyazaki M, Ishikura H. Possible involvement of persistent activity of the mammalian target of rapamycin pathway in the cisplatin resistance of AFP-producing gastric cancer cells. Cancer Biol Ther 2007;6:1036–43.
26. Son J, Lyssiotis CA, Ying H, Wang X, Hua S, Ligorio M, et al. Glutamine supports pancreatic cancer growth through a KRAS-regulated metabolic pathway. Nature 2013;496:101–5.
27. Gorrini C, Harris IS, Mak TW. Modulation of oxidative stress as an anticancer strategy. Nat Rev Drug Discov 2013;12:931–47.
28. Peters JM, Shah YM, Gonzalez FJ. The role of peroxisome proliferator-activated receptors in carcinogenesis and chemoprevention. Nat Rev Cancer 2012;12:181–95.
29. Reynolds MR, Clem BF. Troglitazone suppresses glutamine metabolism through a PPAR-independent mechanism. Biol Chem 2015;396:937–47.